

Resonant x-ray scattering study of layered TbBaCo₂O_{5.5}J. Blasco,^{1,*} J. García,¹ G. Subías,¹ H. Renevier,² M. Stingaciu,³ K. Conder,³ and J. Herrero-Martín⁴¹*Instituto de Ciencia de Materiales de Aragón, CSIC-Universidad de Zaragoza, Departamento de Física de la Materia Condensada, Pedro Cerbuna 12, 50009 Zaragoza, Spain*²*Laboratoire des Matériaux et du Génie Physique, UMR5628, Grenoble INP-MINATEC, 3, parvis L. Néel-BP257, 38016 Grenoble Cedex 1, France*³*Paul Scherrer Inst., Lab. Dev.&Methods, CH 5232 Villigen, Switzerland*⁴*European Synchrotron Radiation Facility, Boîte Postale 220, Grenoble Cedex 38042, France*

(Received 17 April 2008; published 28 August 2008)

Resonant x-ray scattering (RXS) experiments have been performed at the Co *K* edge in the TbBaCo₂O_{5.5} sample. Linear scans in the reciprocal space along $[0k0]$ and $[h00]$ directions were carried out at different energies between 350 and 90 K. This temperature range probes the metallic, insulating, ferrimagnetic, and antiferromagnetic phases. No new reflections, either resonant or not, were detected in any phase transition. We have found strong resonances close to the absorption edge energy for $(0k0)$ reflections with *k* odd. These resonances remain almost constant for the different phases. The cusp of the resonant scattering is either up— $(0\ 3\ 0)$ and $(0\ 7\ 0)$ —or down— $(0\ 1\ 0)$ and $(0\ 5\ 0)$ —depending on the *k* value, and this behavior was completely explained in the frame of the crystal structure and the atomic position of the Tb and Ba atoms. The occurrence of the resonant scattering and its azimuthal behavior has been explained in terms of the anisotropy of the tensor of susceptibility (ATS reflections). RXS comes from the presence of two different environments for the Co ions, octahedra and pyramids of oxygens, ordered along the *b* axis. No evidence for further contributions, such as an orbital ordering, has been found in these experiments in the insulating low temperature phase.

DOI: 10.1103/PhysRevB.78.054123

PACS number(s): 61.05.cf, 71.30.+h, 78.70.Dm, 78.70.Ck

I. INTRODUCTION

Cobalt oxides with the perovskite structure have been intensively investigated the last decades due to the occurrence of new properties arising from an additional degree of freedom: the electronic configuration of the cobalt ion.¹⁻³ Recently, the interest has been focused on layered cobaltites, RBaCo₂O_{5+ δ} with *R*=rare-earth, where coupled transitions (structural, spin, and orbital orderings) have been reported.^{4,5}

When $\delta=0.5$, the formal Co valence is +3 and the compounds show a double perovskite structure as indicated in the Fig. 1. There is an R/Ba ordering along the *c* axis and oxygen vacancies ordering along the *b* axis. This gives rise to the linkage of CoO₆ octahedra and CoO₅ pyramids with Co³⁺ present in the two environments. Competitive (crystal field, on-site Coulomb correlations or intra-atomic exchange) interactions results in three possible spin states for Co³⁺ ions: the low spin state (LS, $t_{2g}^6 e_g^0$), the intermediate spin state (IS, $t_{2g}^5 e_g^1$), and the high spin state (HS, $t_{2g}^4 e_g^2$), which leads to a rich variety of electronic and magnetic transitions as a function of temperature. In particular, TbBaCo₂O_{5.5} exhibits a metal-to-insulator (MI) transition at $T_{MI} \sim 340$ K. On cooling below T_{MI} , the material exhibits a paramagnetic to ferrimagnetic transition at $T_C \sim 280$ K with a spontaneous magnetic moment that disappears at $T_N \sim 250$ K, where an antiferromagnetic phase is formed.⁶ With further cooling, a spin reorientation is realized at $T_S \sim 180$ K.

It is thought that these transitions are accompanied by changes either in the unit cell symmetry or in the cobalt spin state. However, the exact magnetic structure is subject of controversy and four magnetic structures have been suggested for RBaCo₂O_{5.5} compounds.⁶⁻⁹ In the case of TbBaCo₂O_{5.5}, Plakhty *et al.*⁶ proposed the following sequence of magnetic phases in accordance to the space groups: $Pm\bar{3}m(T \geq 255\text{ K}) \rightarrow Pm\bar{3}m(255\text{ K} \geq T \geq 180\text{ K}) \rightarrow Pcca(T \leq 180\text{ K})$. The $Pm\bar{3}m$ phase has the unit cell $a_p \times 2a_p \times 2a_p$, a_p being the primitive cubic cell parameter. The doubling of *c* and *b* axes corresponds to the aforementioned Tb/Ba and oxygen vacancies ordering (see Fig. 1). The $Pm\bar{3}m$ and $Pcca$ phases have $2a_p \times 2a_p \times 2a_p$ and $2a_p \times 2a_p \times 4a_p$ lattice parameters, respectively. In these phases, both type of Co ions (hereafter denoted as Co_{pyr} and Co_{oct} for pyramidal and octahedral coordination, respectively) show magnetic moment. However, M. Soda *et al.*⁹ claims for the

quency of magnetic phases in accordance to the space groups: $Pm\bar{3}m(T \geq 255\text{ K}) \rightarrow Pm\bar{3}m(255\text{ K} \geq T \geq 180\text{ K}) \rightarrow Pcca(T \leq 180\text{ K})$. The $Pm\bar{3}m$ phase has the unit cell $a_p \times 2a_p \times 2a_p$, a_p being the primitive cubic cell parameter. The doubling of *c* and *b* axes corresponds to the aforementioned Tb/Ba and oxygen vacancies ordering (see Fig. 1). The $Pm\bar{3}m$ and $Pcca$ phases have $2a_p \times 2a_p \times 2a_p$ and $2a_p \times 2a_p \times 4a_p$ lattice parameters, respectively. In these phases, both type of Co ions (hereafter denoted as Co_{pyr} and Co_{oct} for pyramidal and octahedral coordination, respectively) show magnetic moment. However, M. Soda *et al.*⁹ claims for the

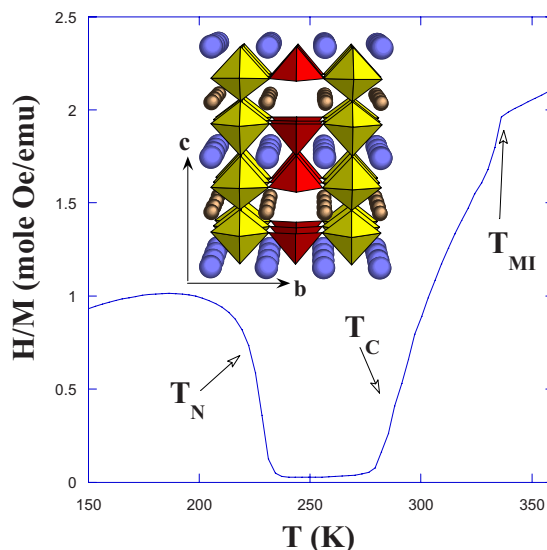


FIG. 1. (Color online) Inverse of magnetization vs temperature for $H=1$ kOe. The arrows indicate the main phase transitions. Inset: Detail of the crystallographic structure of TbBaCo₂O_{5.5}.

presence of a noncollinear structure with the existence of low-spin Co^{3+} sites and Pmmm space group.

The other striking feature observed in these compounds is the metal-insulator transition. Some authors found a significant Jahn-Teller-type distortion in the insulating phase, suggesting a d_{3x-r}^2/d_{3y-r}^2 -type orbital ordering alternation along the b axis as the driving force for the metal-insulator transition, coupled to a spin-state transition from IS (insulating) to HS (metallic).¹⁰ Other authors rule out this orbital ordering as the origin of the insulator to metal transition, which is attributed to a low to high spin transition only in octahedra.⁵ Finally, recent structural refinements have found a spread of Co-O distances, suggesting a more complicated anisotropic distribution for the electronic density around Co_{pyr} and Co_{oct} .⁶

Resonant x-ray scattering (RXS) is a powerful technique widely used to analyze structural and electronic ordered phases.^{11–13} This technique measures the intensity of reflections as a function of photon energy across an absorption edge since the resonant scattering process is sensitive to any anisotropy of the empty electronic levels around the absorbing atom giving rise to a tensorial character for the atomic scattering factor (ASF). The crystal scattering amplitude is then the sum, over all the absorbing atoms in the unit cell, of each ASF. Thus, the appropriate reflections are either forbidden by crystal symmetry or allowed with very low intensity. In these cases, the usually dominant scalar Thomson scattering almost vanishes and strong resonances may arise from the differences between the ASF of the resonant atoms in the cell.

In this paper we report RXS at the Co K edge of the $\text{TbBaCo}_2\text{O}_{5.5}$ sample at different temperatures to probe the type of electronic anisotropy in the different phases. The meaningful reflections to observe differences between Co_{pyr} and Co_{oct} are the $(0k0)$ reflections with odd k (hereafter we refer to the high-temperature phase Pmmm with $a_p \times 2a_p \times 2a_p$ unit cell). For these reflections, the structure factor is proportional to $f(\text{Co}_{\text{pyr}}) - f(\text{Co}_{\text{oct}})$, f being the ASF. This subtraction is null for a Thomson scattering but strong resonances might appear in the vicinity of the Co K edge due to the existence of differences between the two Co sites as charge segregation, orbital ordering, or anisotropy coming from the different local structure.^{14,15}

In order to identify small structural changes, we have performed linear scans along the $[0k0]$ and $[h00]$ directions at different photon energies and at different temperatures across the mentioned phase transitions. We have also measured the resonant intensities of the superlattice reflections such as (010) , (030) , (050) , and (070) as a function of incident energy, azimuthal angle, and temperature. Our results reveal the existence of strong resonances at the Co K edge whose origin is the ordering of oxygen vacancies. We have not found any evidence for an orbital ordering of $d_{3x^2-r^2}/d_{3y^2-r^2}$ -type at the insulator-to-metal transition.

II. EXPERIMENTAL DETAILS

Polycrystalline $\text{TbBaCo}_2\text{O}_{6-\delta}$ was prepared by a solid state reaction. Starting materials of Tb_4O_7 , Co_3O_4 , and

BaCO_3 with 99.99% purity were mixed and ground, followed by heat treatment at 1000–1200 °C in air during at least 100 h with several intermediate grindings. Phase purity of the synthesized compound was checked with conventional x-ray diffractometer (SIEMENS D500). The resulting powder was hydrostatically pressed in the form of rods (8 mm in diameter and ~ 60 mm in length). The rods were subsequently sintered in air at 1230 °C during 20 h in order to obtain the highest possible density of the material (85% of the x-ray density).¹⁶

The crystal growth was carried out using Optical Floating Zone Furnace (FZ-T-10000-H-IV-VP-PC, Crystal System Corp., Japan) with four 300-W halogen lamps as a heat source. The growing conditions were the following: The growth rate was 0.5 mm/h, both rods (feeding and seeding rod) were rotated at about 15 rpm in opposite directions to ensure the liquid homogeneity, 5.5 bar pressure of oxygen (2%) and argon mixture was applied during growing.¹⁶ A few crystals were separated from the as-grown chunk of material and they were finally annealed in oxygen atmosphere for 90 h. (1 bar, 600 °C). Oxygen content was measured by iodometric titration and was found to be 5.48 ± 0.01 .

A crystal was cut and polished to have a flat $(0\ 1\ 0)$ plane. The crystal was twinned so we observed both $[h00]$ and $[0k0]$ domains. A crystal piece was ground and characterized by means of x-ray powder diffraction. The pattern at room temperature completely agrees with previous reports.^{6,9}

The magnetic properties were studied using a commercial Quantum Design superconducting quantum interference device (SQUID) magnetometer. Temperature dependence of the magnetization at $H=1$ KOe was measured with the magnetic field perpendicular to the c direction. The results, in agreement with previous publications,^{6,9,17} are displayed in the Fig. 1. An anomaly in the slope at around 340 K reveals the value of T_{MI} , whereas the ferrimagnetic and antiferromagnetic transition are clearly recognizable in this picture at about 280 and 240 K, respectively.

RXS experiments were performed on the BM2-D2AM beam line of the European Synchrotron Radiation Facility (ESRF) in Grenoble, France.^{18,19} The incident beam was monochromatized by a double crystal Si (111) located between two focusing mirrors. The typical energy resolution of the incident beam at the Co K edge was 1 eV with nearly 100% of linear polarization perpendicular to the vertical scattering plane (σ incident geometry). The sample was mounted with silver paint in a closed cycle refrigerator, which could be rotated about the scattering vector to perform azimuthal scans in a range of $\sim 130^\circ$. The measurements were carried out at selected temperature (90, 200, 250, 300, and 350 K) to probe the different phases existing in this sample. No polarization analysis of the scattered beam was performed so that we have contributions from both $\sigma \rightarrow \sigma'$ and $\sigma \rightarrow \pi'$ channels. The energy dependence of the intensity at the maximum of the diffraction peak was measured for $(0\ 1\ 0)$, $(0\ 3\ 0)$, $(0\ 5\ 0)$, and $(0\ 7\ 0)$ reflections. Corrections for the size of the footprint and intensity variation of the incident beam and absorption were applied.

III. RESULTS AND DISCUSSION

XRS experiments were carried out with the scattering vector Q perpendicular to the ac plane. The crystal was

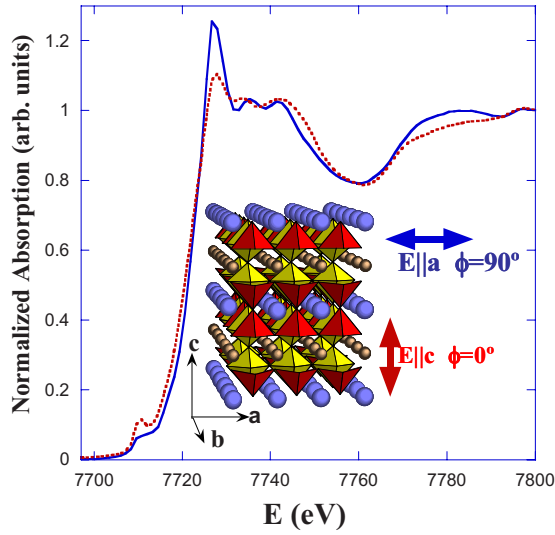


FIG. 2. (Color online) Normalized absorption spectra of $\text{TbBaCo}_2\text{O}_{5.5}$ measured in the fluorescence mode. Continuous line and dotted line refer to the spectrum collected with the electric field parallel to the a axis and c axis, respectively. Inset: Detail of the structure projected on the ac plane and showing the two configurations of the electric field.

mounted as follow: The electrical field (\mathbf{E}) of the polarized beam was parallel to the a axis for the 90° azimuthal angle (ϕ), whereas \mathbf{E} was parallel to the c axis for $\phi=0^\circ$. The inset of Fig. 2 shows in detail both geometrical configurations. Absorption spectra at Co K edge were collected in fluorescence mode for both, $\phi=0^\circ$ and $\phi=90^\circ$, configurations, and the results are also displayed in the Fig. 2. The spectra show differences in the lineshape and energy position of the absorption edge. For $\mathbf{E}\parallel\mathbf{a}$ spectrum, the edge appears to be shifted by ~ 1 eV toward higher energies while it shows a stronger white line and a weaker pre-edge feature. These differences are likely to be ascribed to the strong structural anisotropy, mainly due to the presence of ordered oxygen vacancies. Hence, the $\mathbf{E}\parallel\mathbf{a}$ configuration probes the equatorial local structure of both Co_{pyr} and Co_{oct} . In this case, the local structure is quite similar because both ions show a square coordination in this plane. However, the $\mathbf{E}\parallel\mathbf{c}$ configuration probes the apical local structure that it is quite different for both Co ions. Co_{oct} is surrounded by a square of oxygens while Co_{pyr} is only coordinated to three oxygens (triangle) due to the vacancy of one of the apical oxygens (see Fig. 2).

Linear scans were performed along the $[0k0]$ direction at different energies as a function of temperature on cooling down across the metal to insulator and the spin-ordering transitions. Figure 3(a) shows the scans measured in the insulating phase at $\phi=0^\circ$ [assigned to an orbital-ordering by some authors (Ref. 10)] for three energies: below, at the pre-edge, and at the white line of the absorption spectrum. We observe the same patterns no matter the energy of the incident beam. Similar results were obtained for $\phi=90^\circ$. This result implies that both types of $(0k0)$ reflections with k either even or odd are allowed by symmetry. No new reflections were detected even at the threshold energy. Figure 3(b) shows selected patterns collected at different temperatures

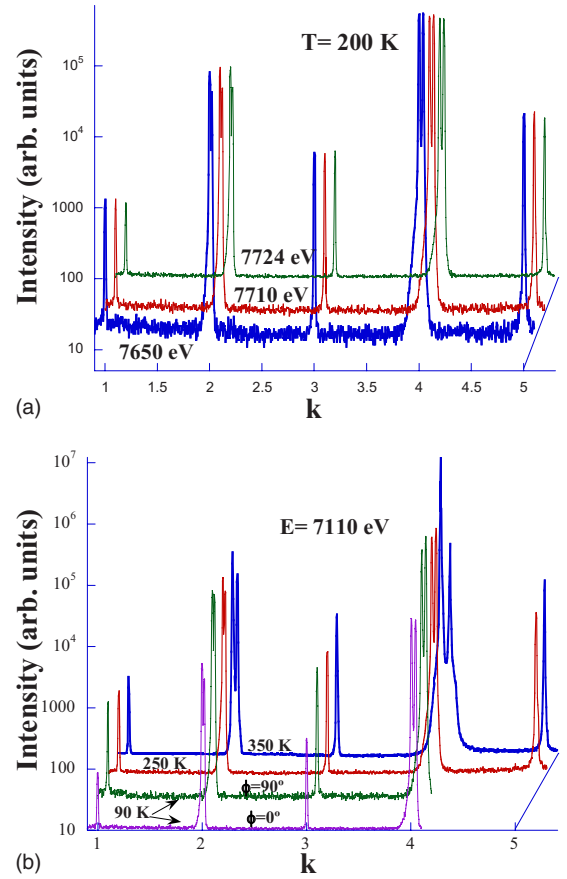


FIG. 3. (Color online) Reciprocal lattice scans along the $[0k0]$ direction. Panel (a): Patterns collected at 200 K with $\phi=0^\circ$ and at different energies, on and out of resonance. Panel (b): Patterns measured $E=7110$ eV (pre-edge energy) with $\phi=0^\circ$ except the curve indicated in the figure. Temperatures are also given for each curve. The patterns have been shifted upward and to the right for the sake of clarity.

between 90 and 350 K. There are no noticeable changes among these patterns too. This result discards the appearing of new periodicity for the low-temperature unit cell. All the patterns reveal split peaks for $(0k0)$ reflections with even k , whereas $(0k0)$ reflections with odd k show a single peak. The splitting of the formers are due to the crystal twinning showing $(h00)$ and $(0k0)$ domains. The absence of $(h00)$ peaks with odd h arise from the crystal symmetry: the a axis is not doubled at high temperature and if it were doubled below T_{MI} , the proposed space groups,⁶ which contains an a -glide plane perpendicular to c axis, only allows $(h00)$ reflections with h even. It is noteworthy that the absence of $(h00)$ reflections with odd h , on resonance at the Co K edge, suggests the absence of significant differences in the local structure between two Co_{pyr} on one hand, and between two Co_{oct} on the other. Thereby, the reported phase transitions below the MI transition (at 255 or 185 K) should have only a magnetic origin.⁶

We are going now to focus in detail on the $(0k0)$ reflections with k odd. Figures 4(a) and 4(b) show the raw-energy-dependent scans of $(0\ 1\ 0)$ and $(0\ 3\ 0)$ reflections, respectively, at different ϕ . Both reflections exhibit resonances

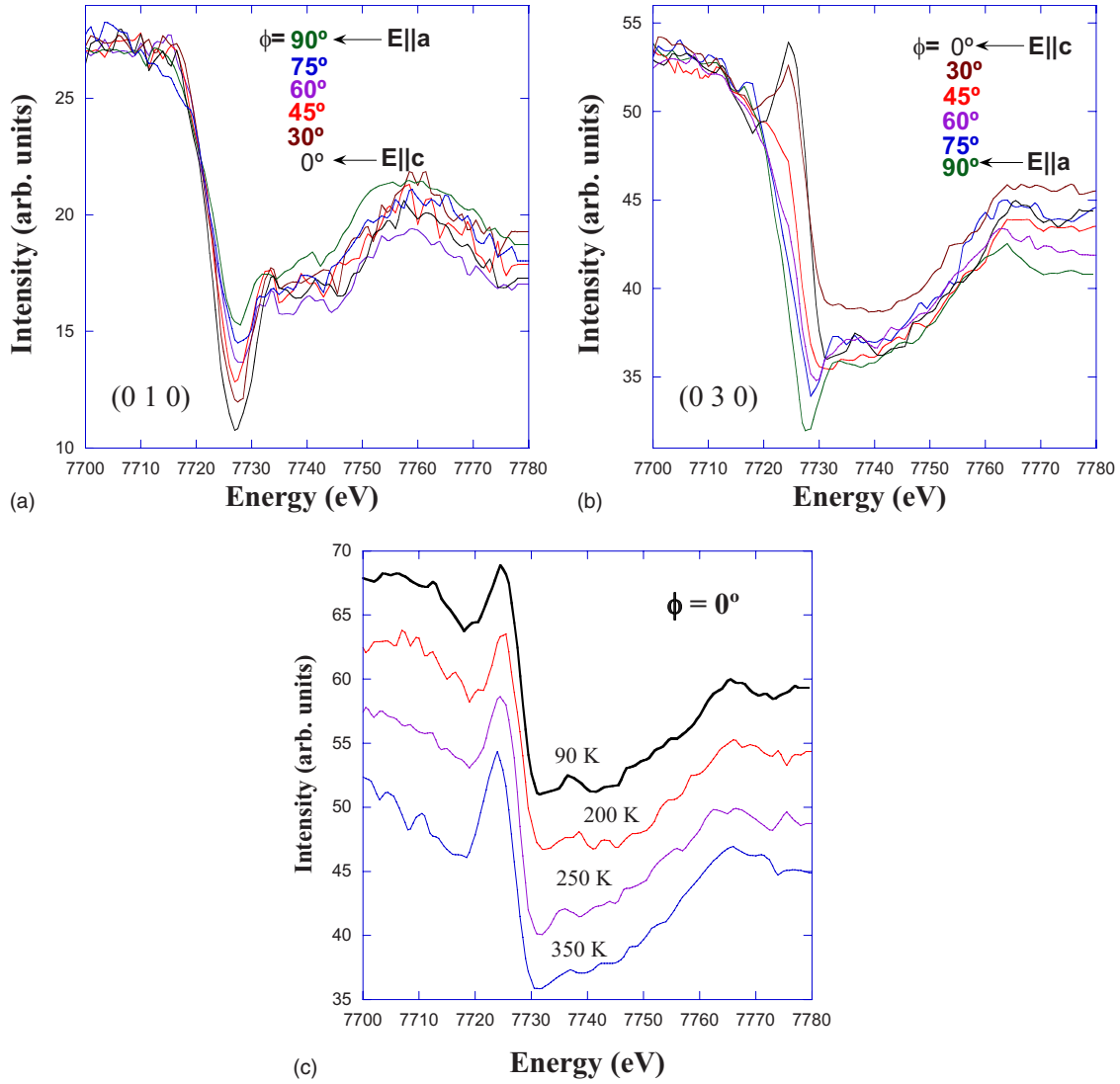


FIG. 4. (Color online) Energy-dependent scans collected at 90 K for the (0 1 0) and (0 3 0) reflections (panel *a* and *b*, respectively) at the azimuthal angles indicated in the figures. Panel *c*: Energy-dependent scans for the (0 3 0) reflections at $\phi=0^\circ$ at the temperatures indicated in the figure. The spectra are shifted upwards for the sake of clarity.

close to the Co absorption *K* edge. These resonances strongly depend on the azimuthal angle reaching the maximum and minimum value at $\phi=0^\circ$ and 90° , respectively. The data were collected at 90 K but similar results were obtained for all temperatures as can be observed in Fig. 4(c) for the (030) reflection, suggesting minor changes among the different phases.

The most striking result is the different behavior of the resonances depending on **Q**. The cusp of the resonant scattering is up for (0 3 0) reflection, giving rise to a strong maximum at 7724.5 eV for $\phi=0^\circ$. The opposite behavior is found for the (0 1 0) reflection, where a minimum is observed at 7727 eV for the same azimuthal angle. We have observed that (0 5 0) and (0 7 0) reflections behave as (0 1 0) and (0 3 0), respectively, in agreement with a main dipolar contribution.

Figure 5 shows the resonance in detail for both reflections at $\phi=0$ and $\phi=90^\circ$ after correcting for absorption by multiplying the raw spectrum by 2μ with μ the linear absorption

coefficient. This correction was performed starting from the average experimental absorption spectrum of Fig. 1. We have calculated the photoelectric cross section, making use of the XCOM tool²⁰ and multiplying by the crystallographic density in order to obtain the linear absorption coefficient. Figure 5 shows that resonance practically disappears at $\phi=90^\circ$, the minimum for both reflections. The nonresonant intensity is characteristic of an allowed Bragg reflection and concurs with the conventional Thomson scattering that is independent of the photon energy.

According to the crystallographic data,⁶ the normal structure factor for these reflections at low temperature, Thomson scattering, is (in number of electrons)

$$F_{th}(0\ 1\ 0) = 2 \times [f_0(\text{Co}_{pyr}) - f_0(\text{Co}_{oct})] - 0.12 \times f_0(\text{Tb}) - 0.05 \times f_0(\text{Ba}) - 0.68 \times f_0(\text{O}) = -16.4$$

and

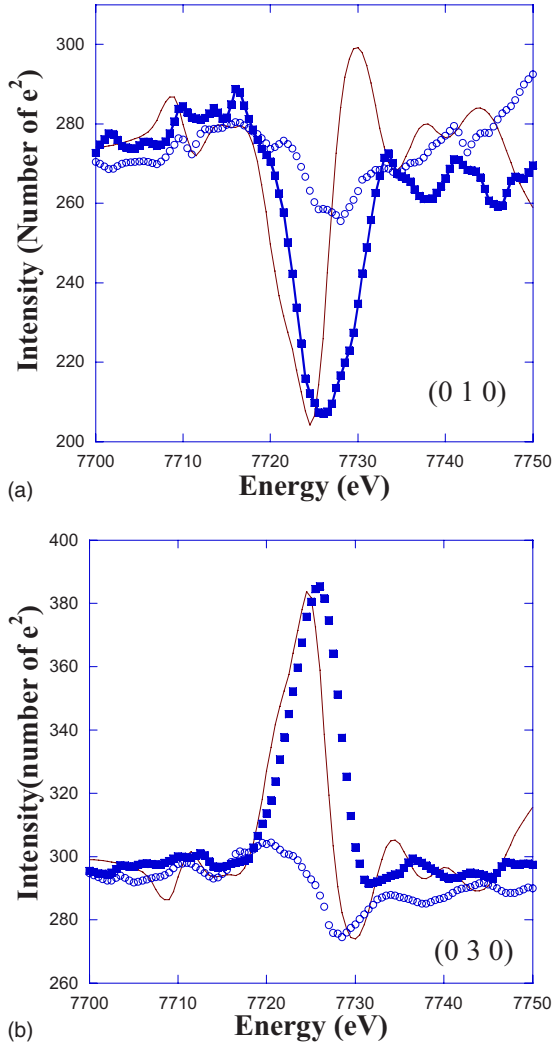


FIG. 5. (Color online) Intensity of (a) the (0 1 0) and (b) the (0 3 0) reflections vs photon energy at $\phi=0^\circ$ (squares) and $\phi=90^\circ$ (circles) together with the simulated RXS spectra (continuous line).

$$F_{\text{Th}}(0\ 3\ 0) = 2 \times [f_0(\text{Co}_{\text{pyr}}) - f_0(\text{Co}_{\text{oct}})] + 0.37 \times f_0(\text{Tb}) \\ + 0.15 \times f_0(\text{Ba}) - 1.48 \times f_0(\text{O}) = +17.3.$$

Contributions from Co ions are null for the Thomson scattering assuming the same formal +3 valence for both ions. It is noteworthy that the different sign of the structure factor for both reflections mainly comes from the atomic displacement of Tb and Ba ions from the ideal tetragonal position. This fact does not affect the nonresonant intensity— $I = F(hkl) \times F^*(hkl)$ —but it will determine the anomalous behavior as we will see later.

The occurrence of the resonance at energies close to the Co *K* edge indicates that the main contribution comes from the angular dependence of the absorption spectra²⁰ due to the different local structure between Co_{pyr} and Co_{oct} as can be inferred from Fig. 2. The strong azimuthal dependence derives from this anisotropy of the absorption spectra and consequently from the anisotropy of the anomalous ASF of Co atoms. At the Co *K* edge, the structure factor includes the anomalous contribution arising from the resonant atoms and then, $F(0k0) = F_{\text{Th}}(0k0) + 2 \times [f \text{Co}_{\text{pyr}}(E) - f \text{Co}_{\text{oct}}(E)]$, where

$f(E)$ is generally represented by $f'(E) + if''(E)$, depending on the x-ray energy (E) with f' and f'' the real and imaginary parts of the anomalous scattering factor, respectively. For dipole transitions, the anomalous scattering factor is a tensor of rank two that is expressed in the crystallographic frame in the following.

The point symmetry for both Co sites is C_{2v} in the Pmmn unit cell. As a first approximation, we consider a regular octahedron and hence, we approach the point symmetry for Co_{oct} as O_h , and the anomalous ASF behaves as scalar with similar tensor components with respect to the three crystallographic axes (denoted as f_b).²¹ On the other hand, Co_{pyr} has been approached as a perfect pyramid (C_{4v} point symmetry) and the scattering tensor has two different components, two equal in the basal plane (denoted as f_a) and the other along the axis of the pyramid (denotes as f_c). It is noteworthy that the principal axes of the tensor coincide with the crystallographic axes in the present case. In this way, the anomalous scattering tensor is

$$f(\text{Co}_{\text{pyr}}) - f(\text{Co}_{\text{oct}}) = \begin{pmatrix} f_a & 0 & 0 \\ 0 & f_a & 0 \\ 0 & 0 & f_c \end{pmatrix} - \begin{pmatrix} f_b & 0 & 0 \\ 0 & f_b & 0 \\ 0 & 0 & f_b \end{pmatrix} \\ = \begin{pmatrix} f_a - f_b & 0 & 0 \\ 0 & f_a - f_b & 0 \\ 0 & 0 & f_c - f_b \end{pmatrix}.$$

The intensity of the scattering signal usually exhibits polarization and azimuthal properties because both the incident and diffracted polarizations depend on the azimuthal crystal setting.^{12,15,17,22} Thereby, the vectors for the polarization channels are described as a function of the Bragg angle θ and the azimuth angle ϕ as

$$\sigma(0k0) = \sigma'(0k0) = (\sin \phi \ 0 \ \cos \phi),$$

$$\pi'(0k0) = (-\sin \theta \ \cos \phi \ \cos \theta \ \sin \theta \ \sin \phi),$$

where σ' and π' refer to the scattered polarization vectors perpendicular and parallel to the diffraction plane (the incident light only has the parallel component, σ). Therefore, the anomalous structure factor for the $\sigma \rightarrow \sigma'$ channel is

$$F_{\sigma \rightarrow \sigma'}(0k0) = (\sin \phi \ 0 \ \cos \phi) \begin{pmatrix} f_a - f_b & 0 & 0 \\ 0 & f_a - f_b & 0 \\ 0 & 0 & f_c - f_b \end{pmatrix} \\ \times \begin{pmatrix} \sin \phi \\ 0 \\ \cos \phi \end{pmatrix} = (f_a - f_b) + (f_c - f_a) \cos^2 \phi$$

and for the $\sigma \rightarrow \pi'$ channel:

$$F_{\sigma \rightarrow \pi'}(0k0) = (\sin \phi \ 0 \ \cos \phi) \begin{pmatrix} f_a - f_b & 0 & 0 \\ 0 & f_a - f_b & 0 \\ 0 & 0 & f_c - f_b \end{pmatrix} \\ \times \begin{pmatrix} -\sin \theta \cos \phi \\ \cos \phi \\ \sin \theta \sin \phi \end{pmatrix} \\ = (f_c - f_a) \cos \phi \sin \phi \sin \theta.$$

Taking into account that Co-O bonds are very similar for equatorial Co_{oct} and Co_{pyr} and the projected symmetry in the *ab* plane is the same (square base), we can assume $f_a = f_b$ and the previous expressions result in $F_{\sigma \rightarrow \sigma'}(0k0) = 2(f_c - f_b) \cos^2 \phi$ and $F_{\sigma \rightarrow \pi'}(0k0) = 2(f_c - f_b) \cos \phi \sin \phi \sin \theta$.

The intensities of the resonant reflections are given by Eq. (1):

$$I_{\sigma \rightarrow \sigma'}(010) = [-16.4 + 2(f'_c - f'_b) \cos^2 \phi + 2i(f''_c - f''_b) \cos^2 \phi]^2 \\ = 269 - 65.6(f'_c - f'_b) \cos^2 \phi + 4(f'_c - f'_b)^2 \cos^4 \phi \\ + 4(f''_c - f''_b)^2 \cos^4 \phi,$$

$$I_{\sigma \rightarrow \sigma'}(030) = [17.3 + 2(f'_c - f'_b) \cos^2 \phi + 2i(f''_c - f''_b) \cos^2 \phi]^2 \\ = 299 + 69.2(f'_c - f'_b) \cos^2 \phi + 4(f'_c - f'_b)^2 \cos^4 \phi \\ + 4(f''_c - f''_b)^2 \cos^4 \phi.$$

The sign of the Thomson scattering determines the up (positive) or down (negative) contribution from the resonant scattering. The $\sin^2 \phi \cos^2 \phi$ factor implies that $\sigma \rightarrow \pi'$ channel is null for $\phi = 0^\circ$ and 90° . Its maximum contribution is achieved for $\phi = 45^\circ$ but due to the $\sin^2 \theta$ factor, it values 0.04 and 0.36 of the $\sigma \rightarrow \sigma'$ channel for the (010) and (030) reflections, respectively.

In order to evaluate the intensity of both types of resonant reflections, we have made use of the polarized absorption spectra from Fig. 1. Bearing in mind that the energy dependence of the anomalous atomic scattering factor is given by $f(E) = f'(E) + if''(E)$. The imaginary part is related to the linear absorption coefficient through the optical theorem by $f''(E) = (mcE/2e^2h)\mu(E)$. The real part $f'(E)$ is calculated through the Kramers-Kronig transformation of $f''(E)$, where Cromer and Liberman calculation²³ was applied to estimate the region outside the absorption measurements. In order to get the distinct components of the anomalous atomic scattering factor, we have made the assumption that $\mu(E)$ measured for $\mathbf{E} \parallel \mathbf{a}$ gives the imaginary part coming from the square coordination (f''_b coefficient), whereas $\mu(E)$ measured for $\mathbf{E} \parallel \mathbf{c}$ is composed by square and triangle components so the f''_c factor arises from $2 \times [\mu(\mathbf{E} \parallel \mathbf{c}) - 1/2\mu(\mathbf{E} \parallel \mathbf{a})]$.

Figure 5 shows the simulated RXS spectra drawn from the previous model at $\phi = 0^\circ$, near the maximum intensity. The experimental data was normalized out of the resonance to the Thomson scattering for the sake of comparison. We observe that our model qualitatively reproduces the shape and intensity of the resonance for the two reflections. We have also observed that the second order terms in Eq. (1),

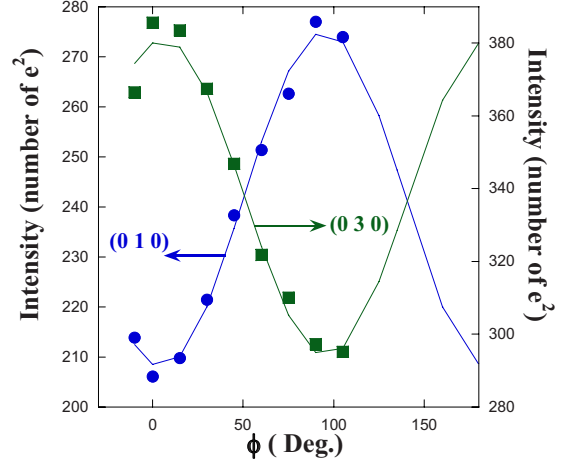


FIG. 6. (Color online) Azimuthal behavior of the scattered intensity at the resonance energy for (0 1 0) and (0 3 0) reflections. The lines are fits to the expression $I = a + b \cos^2(\phi + c)$. For the (0 1 0) reflection, we obtain the values: $a = 275 \pm 2$; $b = 67 \pm 2$; $c = -4 \pm 2$ and for the (0 3 0) reflection: $a = 294 \pm 3$; $b = 87 \pm 4$; $c = -6 \pm 2$.

such as $(f'_c - f'_b)^2$ and $(f''_c - f''_b)^2$, can be neglected to reproduce the resonance. In this way, the azimuthal behavior can be approximated for the $\sigma \rightarrow \sigma'$ channel as $I(010) = 269 - 65.6(f'_c - f'_b) \cos^2 \phi$ and $I(030) = 299 + 69.2(f'_c - f'_b) \cos^2 \phi$. Figure 6 shows the azimuthal dependence of the resonant intensities for both reflections. The data fit quite well to a $A + B \cos^2(\phi + C)$ function, in agreement with the main contribution of the $\sigma \rightarrow \sigma'$ channel. The fitted parameters nicely agree with the abovementioned calculated expression for this $\sigma \rightarrow \sigma'$ channel, suggesting a minor contribution from the $\sigma \rightarrow \pi'$ channel. We note here, that this simplified model accounts nicely with the experimental data, indicating that only the anisotropy of the Co_{pyr} is responsible for the observed resonances.

At this point, one can wonder about the role of an orbital ordering in these resonant spectra. Resonant scattering at the (0*k*0) reflections would be expected for the orbital ordered pattern displayed in the Fig. 1 of Ref. 10. It is easy to deduce that the strongest resonance would appear for $\mathbf{E} \parallel \mathbf{a}$ while a minimum occurs for $\mathbf{E} \parallel \mathbf{c}$ (parallel orbitals). The azimuthal contribution for the linear term of the structure factor ($\sigma \rightarrow \sigma'$ channel) would be $(f_x - f_y) \sin^2 \phi$, f_x being the atomic factor along the orbital lobe and f_y perpendicular to it, just out of phase of the experimental results ($\pi/2$ phase shift).

IV. CONCLUSIONS

Resonances have been observed at the Co *K* edge for (0*k*0) reflections with *k* odd in the TbBaCo₂O_{5.5} compound. The resonant cusp is up (positive) for both (0 3 0) and (0 7 0) reflections but it is down (negative) for (0 1 0) and (0 5 0) ones. This behavior arises from the crystal structure, specifically from the displacement of Tb and Ba ions from the ideal tetragonal positions. The resonance occurrence and its azimuthal behavior can be explained as coming from the anisotropy of the tensor of susceptibility produced by the ordered

arrangement of oxygen vacancies along the b axis. Reciprocal lattice scans along the $[0k0]$ direction were performed between 90 and 350 K across the insulator to metal transition at different photon energies, on and out of resonance. Neither new reflections nor changes on the energy dependence of the $(0 \text{ odd } 0)$ reflections were detected respect to the high-temperature phase. This result discards differences among Co_{oct} or among Co_{pyr} in the low-temperature insulating phases. Moreover, the absence of $(h00)$ reflections with h odd indicates that reported⁶ structural transitions implying the doubling of the a axis should only have a magnetic origin.

We have not found evidences from further contributions such as an orbital ordering of 3d orbitals in agreement with a neutron study on related Gd-based samples.²⁴

ACKNOWLEDGMENTS

The authors acknowledge financial support from CICYT (Project No. MAT05-04562) and DGA (CAMRADS and PIP018/2005). We also thank ESRF for beam time granting and the D2AM staff for their kind assistance during the experiment. We are also indebted to M. G. Proietti for her kind help in the experiment.

*Corresponding author. Present address: I C M A-Departamento de Física de la Materia Condensada CSIC-Universidad de Zaragoza. C/Pedro Cerbuna 12, 50009 Zaragoza, Spain; jbc@unizar.es

¹M. A. Señaris-Rodríguez and J. B. Goodenough, *J. Solid State Chem.* **118**, 323 (1995).

²M. Takahashi and J. I. Igarashi, *Phys. Rev. B* **55**, 13557 (1997).

³M. R. Ibarra, R. Mahendiran, C. Marquina, B. García-Landa, and J. Blasco, *Phys. Rev. B* **57**, R3217 (1998).

⁴Md. Motin Seikh, Ch. Simon, V. Caignaert, V. Pralong, M. B. Lepetit, S. Boudin, and B. Raveau, *Chem. Mater.* **20**, 231 (2008).

⁵C. Frontera, J. L. García-Muñoz, A. Llobet, and M. A. G. Aranda, *Phys. Rev. B* **65**, 180405(R) (2002).

⁶V. P. Plakhty, Yu. P. Chernenkov, S. N. Barilo, A. Podlesnyak, E. Pomjakushina, E. V. Moskvina, and S. V. Gavrilov, *Phys. Rev. B* **71**, 214407 (2005).

⁷F. Fauth, E. Suard, V. Caignaert, and I. Mirebeau, *Phys. Rev. B* **66**, 184421 (2002).

⁸A. A. Taskin, A. N. Lavrov, and Y. Ando, *Phys. Rev. Lett.* **90**, 227201 (2003).

⁹M. Soda, Y. Yasui, Y. Kobayashi, T. Fujita, M. Sato, and K. Kakurai, *J. Phys. Soc. Jpn.* **75**, 104708 (2006).

¹⁰Y. Moritomo, T. Akimoto, M. Takeo, A. Machida, E. Nishibori, M. Takata, M. Sakata, K. Ohoyama, and A. Nakamura, *Phys. Rev. B* **61**, R13325 (2000).

¹¹J. L. Hodeau and H. Renevier, *Neutron and X-Ray Spectroscopy* (Springer, Dordrecht, Netherlands, 2006), pp. 239–269.

¹²J. Herrero-Martín, J. García, G. Subías, J. Blasco, M. C. Sánchez, and S. Stanescu, *Phys. Rev. B* **73**, 224407 (2006).

¹³J. García, G. Subías, M. G. Proietti, H. Renevier, Y. Joly, J. L. Hodeau, J. Blasco, M. C. Sánchez, and J. F. Béjar, *Phys. Rev. Lett.* **85**, 578 (2000).

¹⁴D. H. Templeton and L. K. Templeton, *Acta Crystallogr., Sect. A: Found. Crystallogr.* **42**, 478 (1986).

¹⁵V. E. Dmitrienko, *Acta Crystallogr., Sect. A: Found. Crystallogr.* **40**, 89 (1984).

¹⁶M. Stingaciu, E. Pomjakushina, H. Grimmer, M. Trottmann, and K. Conder, *J. Cryst. Growth* **310**, 1239 (2008).

¹⁷M. Soda, Y. Yasui, T. Fujita, T. Miyashita, M. Sato, and K. Kakurai, *J. Phys. Soc. Jpn.* **72**, 1729 (2003).

¹⁸J. L. Ferrer, J. P. Simon, J. F. Berar, B. Caillot, E. Fanchon, O. Kaikati, S. Arnaud, M. Guidotti, M. Pirochi, and M. Roth, *J. Synchrotron Radiat.* **5**, 1346 (1998).

¹⁹H. Renevier, S. Grenier, S. Arnaud, J. F. Béjar, B. Caillot, J. L. Hodeau, A. Letoublon, M. G. Proietti, and B. Ravel, *J. Synchrotron Radiat.* **10**, 435 (2003).

²⁰Available at the web site <http://physics.nist.gov/PhysRefData/contents.html>

²¹C. Brouder, *J. Phys.: Condens. Matter* **2**, 701 (1990).

²²J. Herrero-Martín, J. García, G. Subías, J. Blasco, and M. Concepción Sánchez, *Phys. Rev. B* **70**, 024408 (2004).

²³D. T. Cromer and D. Liberman, *J. Chem. Phys.* **53**, 1891 (1970).

²⁴C. Frontera, J. L. García-Muñoz, A. Llobet, Ll. Mañosa, and M. A. G. Aranda, *J. Solid State Chem.* **171**, 349 (2003).